

# Interindividual Variations in Foveal Anatomy and Artifacts Seen on Inner Retinal Probability Maps from Spectral Domain OCT Scans of the Macula

Carlos Gustavo De Moraes<sup>1</sup>, Hassan Muhammad<sup>2,3</sup>, Khushmit Kaur<sup>4</sup>, Diane Wang<sup>4</sup>, Robert Ritch<sup>5</sup>, and Donald C. Hood<sup>4,6</sup>

<sup>1</sup> Bernard and Shirlee Brown Glaucoma Research Laboratory, Department of Ophthalmology, Edward S. Harkness Eye Institute, Columbia University Medical Center, New York, NY, USA

<sup>2</sup> Department of Physiology, Biophysics, and Systems Biology, Weill Cornell Medicine, New York, NY, USA

<sup>3</sup> Computational and Systems Biology, Memorial Sloan Kettering Cancer Center, New York, NY, USA

<sup>4</sup> Department of Psychology, Columbia University, New York, NY, USA

<sup>5</sup> Einhorn Clinical Research Center, New York Eye and Ear Infirmary of Mount Sinai, New York, NY, USA

<sup>6</sup> Department of Ophthalmology, Columbia University Medical Center, New York, NY, USA

**Correspondence:** Carlos Gustavo De Moraes, Edward S. Harkness Eye Institute, 635 W 165th St, Box 69, New York, NY 10032, USA. e-mail: cvd2109@cumc.columbia.edu

**Received:** 19 September 2017

**Accepted:** 18 December 2017

**Published:** 9 March 2018

**Keywords:** fovea; macula; glaucoma; optical coherence tomography

**Citation:** De Moraes CG, Muhammad H, Kaur K, Wang D, Ritch R, Hood DC. Interindividual variations in foveal anatomy and artifacts seen on inner retinal probability maps from spectral domain OCT scans of the macula. *Trans Vis Sci Tech.* 2018;7(2):4, <https://doi.org/10.1167/tvst.7.2.4> Copyright 2018 The Authors

**Purpose:** We tested the hypothesis that variations in foveal morphology can account for artifacts seen on optical coherence tomography (OCT) retinal ganglion cell (RGC) layer probability maps.

**Methods:** A total of 126 healthy subjects were tested with spectral domain (sd) OCT. Thickness and probability maps of the macular RGC plus inner plexiform layer (RGC+) were obtained with customized software. Macular b-scans were analyzed to derive three foveal anatomic parameters: width, depth, and slope. The distribution of these parameters was compared between eyes with and without circumfoveal artifacts seen in the central 4° of macular RGC+ probability maps.

**Results:** Of 126 healthy subjects, 12 (9.5%) had an abnormal circumfoveal region (artifact) on RGC+ probability maps. Based upon the normal distribution of the three anatomic parameters, only three of the 12 eyes (25%) fell outside the 95% confidence interval of one or more of the three foveal morphologic parameters. Multivariable logistic regression revealed that the parameter slope was significantly associated with the presence of these artifacts (odds ratio = 0.26;  $P = 0.019$ ). However, the combination of these parameters and age explained only 11% of the total variance of these artifacts.

**Conclusions:** Fovea morphology, as measured based upon width, depth, and slope, has a minor role in explaining artifacts seen on macular scans. Variations in the distribution of RGC+ thickness that are not reflected in our measures warrant further investigation as potential sources of artifacts.

**Translational Relevance:** A small proportion of circumfoveal artifacts seen on RGC+ probability maps can be explained by variations in foveal anatomy.

## Introduction

Traditionally, glaucomatous damage to the macula (herewith defined as the central  $\pm 8^\circ$  around the fovea) has been thought to be relatively rare in the early stages of the glaucoma continuum. As such, scrutinized structural and functional assessment of the macula was warranted only in advanced stages.<sup>1</sup>

However, the macula recently has gained increasing attention as a site of early glaucomatous damage,<sup>2,3</sup> which should be monitored for diagnosis<sup>4-8</sup> and progression of glaucoma.<sup>9-11</sup>

One main reason that glaucomatous damage to the macula long has been overlooked is that conventional techniques to detect functional and structural damage, namely 24-2 standard automated perimetry (SAP) and, more recently, circumpapillary retinal nerve fiber

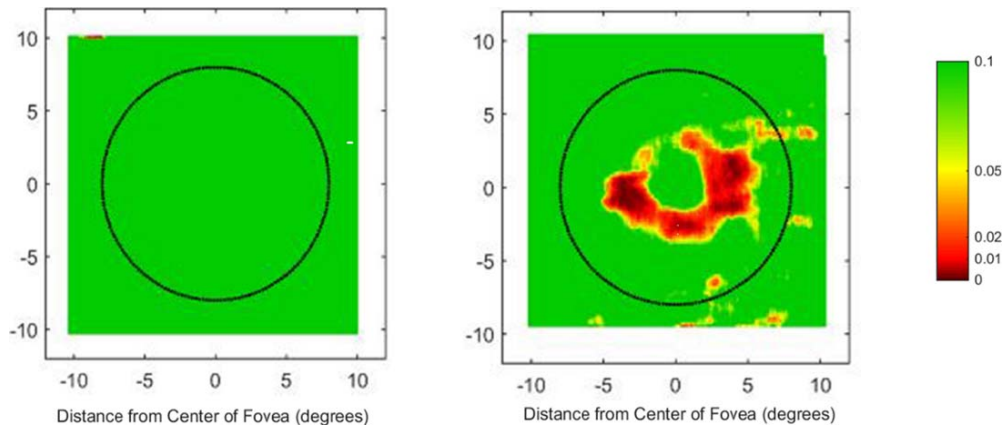


**Figure 1.** RGC+ layer derived from sdOCT cube scans of the macula of healthy subjects without (*left*) and with (*right*) circumfoveal artifacts.

layer (cpRNFL) thickness measured with spectral-domain optical coherence tomography (sdOCT), often miss macular damage.<sup>4–7,12–14</sup> For instance, 24-2 SAP misses 16<sup>12</sup> to 73%<sup>7</sup> of central field defects detected with 10-2 SAP, which tests the central field with higher density of points (16 points at 6° distance vs. 68 points at 2°, respectively). In addition, sdOCT-derived cpRNFL misses 36% to 77% of macular damage detected with 10-2 sdOCT cube scans of macula.<sup>5</sup>

While sdOCT scans of the macula may show better accuracy than conventional cpRNFL, scans, intersubject variability can affect the diagnostic performance of both methods. In the optic disc, for example, disc size and shape,<sup>15</sup> as well as the position of blood vessels,<sup>16</sup> are important covariates to be considered when diagnosing glaucomatous optic neuropathy. In the macula, however, little is known about the sources of variability and how they can influence diagnostic performance.<sup>17–19</sup>

In healthy subjects, apparent circumfoveal abnormalities can be seen on retinal ganglion cell plus inner plexiform (RGC+) probability maps derived from cube scans obtained with sdOCT (Fig. 1). In addition, Sepulveda et al.<sup>20</sup> described differences in foveal shape among healthy subjects that should be taken into account when investigating glaucomatous damage in the macular region. Moreover, the macular RGC+ displacement (relative to the photoreceptors) must be considered when comparing 10-2 data to OCT RGC+ measures,<sup>14,21</sup> and Turpin et al.<sup>22</sup> reported that this displacement can vary among individuals.

We tested the hypothesis that variations in foveal pit morphology can account for artifacts seen around the fovea on RGC+ probability maps. In particular, we evaluated how much of the variance of abnormal RGC+ probability maps is explained by a set of morphologic parameters and age.

## Methods

This prospective, cross-sectional study was approved by the institutional review boards of Columbia University Medical Center and followed the tenets of the Declaration of Helsinki and the Health Insurance Portability and Accountability Act. Written informed consent was obtained from all eligible subjects.

A total of 126 healthy individuals were selected based upon the following inclusion criteria: age 18 years or older (mean = 38.5; SD = 14), a correction between +3.0 and –6.0 diopters (D) spherical, intraocular pressure (IOP) ≤ 21 mmHg, axial length between 22 and 26 mm, a normal clinical examination, including normal optic discs upon review by a glaucoma specialist, and normal visual fields (SITA Standard 24-2 test procedure; Carl Zeiss Meditec, Inc., Dublin, CA). A visual field was defined based upon a Glaucoma Hemifield Test (GHT) within normal limits and a pattern standard deviation (PSD) at  $P > 5\%$ . Reliable visual field required false negative responses and fixation losses ≤ 33% and false positives ≤ 15%. Exclusion criteria included a history of ocular disease or a family history of glaucoma. If both eyes of the same individual were eligible, one eye was selected randomly for the study procedures. These 126 eyes had 6 × 6 mm sdOCT macular cube scans (3D-OCT2000; Topcon, Inc., McAllen, TX) that were free of eye movement and other artifacts.

### RGC+ Probability Map

All participants were scanned using an sdOCT including optic disc- and macula-centered cube scan protocol (6 × 6 mm, 128 horizontal B-scans with 512 A-scans). For our study, only the macula-centered

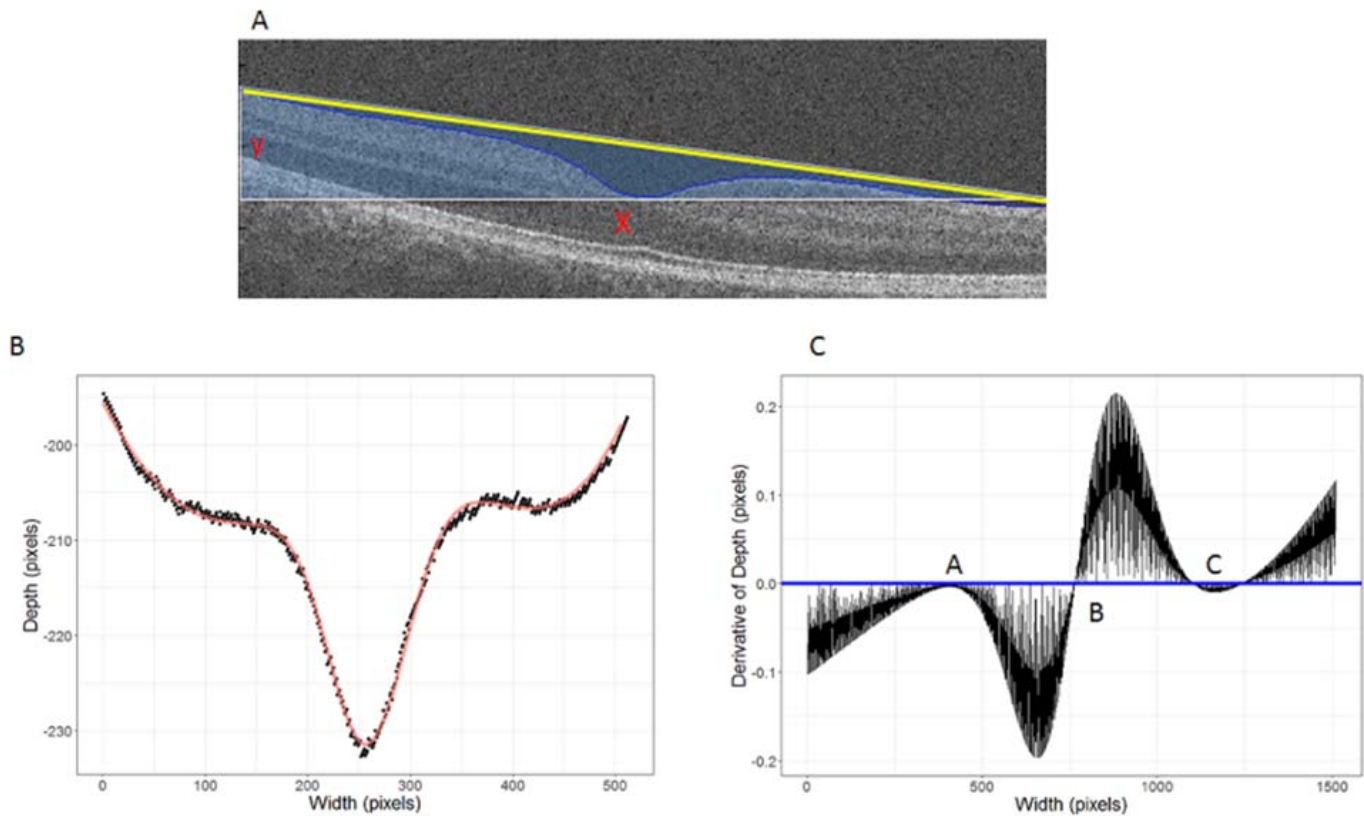


**Figure 2.** Fitting a Gaussian to foveal shape. (A) A fourth-order negative Gaussian was fitted to the border between the inner limiting membrane and vitreous (B). (C) Locations of the foveal center and perifoveal peaks were taken as the locations of the two local maxima (points A and C) and one local minimum (B), respectively, on the first derivative of the Gaussian.

scans were analyzed. The details of this technique have been described previously.<sup>23</sup> In brief, the thicknesses of the RGC+ layer were determined using the sDOCT instrument's software (Topcon, Inc.). Based upon the software's segmentation of the outer border of the RNFL and outer border of the inner plexiform layer, RGC+ thickness maps were created using a custom program in MATLAB (MathWorks, Inc., Natick, MA).<sup>24</sup> Finally, probability maps were generated based upon the 126 healthy individuals using a per-pixel  $z$ -score. Examples of the resulting RGC+ probability map for two healthy individuals are shown in Figure 1. The probabilities corresponding to the pseudo-colors are shown on the calibration bars in Figure 1. The circumfoveal region ( $\pm 4^\circ$  blue circle) was considered abnormal if there were regions falling below the 1% confidence limit (red area) in both hemi-retinas.

### Deriving Foveal Morphologic Parameters

We used a modified version of the methodology described by Dubis et al.<sup>19</sup> to derive objective metrics

of the fovea. In brief, their analysis was based upon the work of Williams,<sup>25</sup> who described that the contour of the foveal pit is well represented by a Gaussian function. However, while this function approximates the shape of the foveal pit, it does not completely capture the rim contour. Identification of the rim contour provides access to the automated measure of pit depth and diameter. Dubis et al.<sup>19</sup> tested several functions for their ability to fit foveal pit contour, and found that a difference of Gaussians (DoG) function provides the best fit to the foveal OCT scans.

First, b-scans corresponding to the horizontal meridian were identified after manually marking the center of the fovea. These scans then were rotated by manually fitting a linear line reference line across the surface of the retina in the b-scan and rotating until angle of incidence was 0. The yellow line in Figure 2A represents the line used for rotation. To extract the various foveal pit metrics (diameter, depth, and slope) automatically, a fourth-order negative Gaussian was fitted to the border between the inner limiting membrane and vitreous (Fig. 2B). This border was

defined as a segmentation line produced by the sdOCT software. Further, this border was hand corrected using previously validated methods.<sup>26</sup> Locations of the foveal center and perifoveal peaks were taken as the locations of the two local maxima (Fig. 2C, points A and C) and one local minimum (point B), respectively, on the first derivative of the Gaussian. The following morphologic parameters were defined:

1. Width (W): Horizontal distance from peak to peak (points A–C, Fig. 2B).
2. Depth (D): Average vertical distances from foveal pit to each peak (B–A and B–C).
3. Slope (S): Steepest slope of each foveal edge.

These parameters have been used previously in studies evaluating foveal morphology in retinal conditions.<sup>27–29</sup>

## Main Outcome Measures

To obtain outcome measures, we: (1) identified how many eyes had an abnormal circumfoveal region in both hemiretinas as defined above; (2) defined 95% confidence limits (CI) of the normative database for each of the three foveal morphologic parameters; (3) evaluated how many of those eyes with an abnormal circumfoveal region had at least one of the three foveal morphologic parameters falling outside the 95% CI limits; and (4) finally, conducted a binary logistic regression analysis testing the relationship between the three foveal parameters, in addition to age, and the odds of having an abnormal circumfoveal region. Statistical analyses were performed using commercially available software (STATA, version 14; StataCorp LP, College Station, TX). Statistical significance was defined at  $P < 0.05$ .

## Results

Consider the RGC+ probability maps for the two healthy eyes in Figure 1. In one case (A), the probability map had no abnormal regions, while in the other eye (B) there was a ring of abnormally thin RGC+ around the foveal center. Of 126 eyes, 12 (9.5%) had an abnormal circumfoveal RGC+ probability map as defined above.

Figure 3 shows the histograms with the distribution of the three anatomic parameters and age for all 126 eyes. In each Figure, the number above the bar refers to the patient number of one of the 12 “abnormal” eyes. For example, in Figure 3A, there

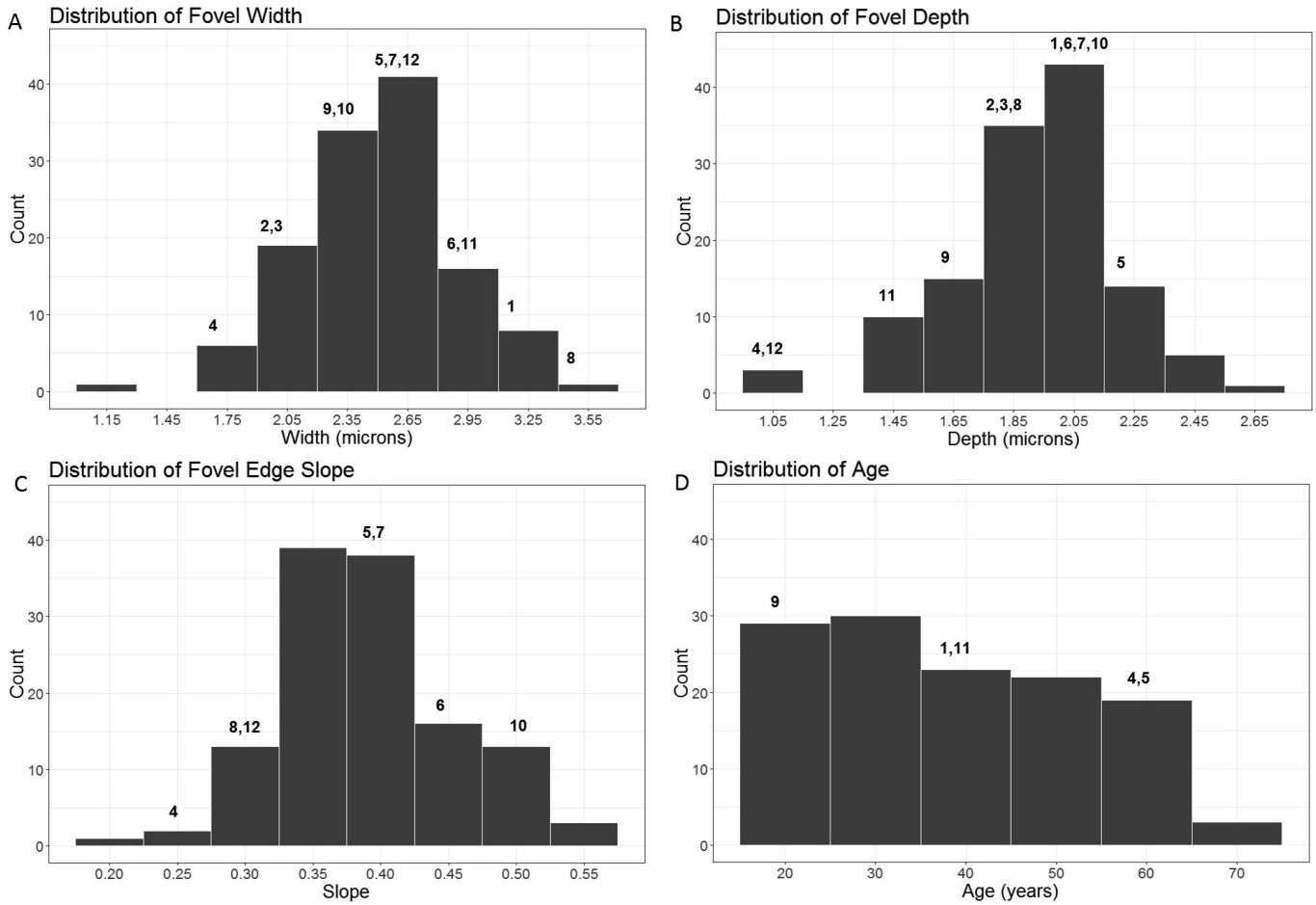
were three eyes (#5, #7, and #12) falling in the bin with the center at 2.65  $\mu\text{m}$ . In general, these 12 eyes were not outliers for the three foveal morphologic parameters (W, D, S), all of which displayed normal distributions for the entire sample of 126. That is, the 12 had parameter values that spanned most of the range. Similarly, eyes with abnormal circumfoveal RGC+ thickness were found throughout the age distribution for the entire sample.

Figure 4 shows the RGC+ probability maps of all 12 eyes with abnormal circumfoveal RGC+ thickness. Only three of the 12 eyes fell outside the 95% CI on one or more of the three foveal morphologic parameters (all three for S and two for W and D). Those three eyes are shown in the bottom row, the values in red depicting outliers for the three parameters. Only two of the 12 eyes fell outside the 95% CI for age. Those two eyes (maps 4 and 5 in Fig. 4) fell above the 95th percentile.

Figure 5 shows the RGC+ probability map (left) and horizontal b-scans (middle) for eyes with normal or abnormal RGC+ thickness and morphologic foveal measurements (right) based upon the 95% CI of the distribution of parameters investigated. Map A shows an eye with normal parameters while Maps B to E show eyes that are outliers for width (B), depth (C), slope (D), and age (E) despite having normal RGC+ maps.

The three parameters were correlated significantly with each other (Pearson’s correlation coefficients,  $r$ ; depth versus width,  $r = 0.3143$ ,  $P = 0.0003$ ; slope versus width,  $r = -0.4865$ ,  $P < 0.0001$ ; depth versus slope,  $r = 0.5141$ ,  $P < 0.0001$ ). However, age was not significantly associated with any of the three parameters (all  $P > 0.175$ ).

A binary logistic regression model was created to determine whether the three predefined parameters were associated with an abnormal RGC+ map. The parameters included foveal width, depth, slope, and the individual’s age. Each parameter was tested individually in univariable models and then combined in a multivariable, stepwise backward-selection model. The results of the univariable and multivariable models are shown in the Table. Note that the coefficients were in the expected direction, that is, abnormal RGC+ maps were more likely with increased width, decreased depth, and decreased slope. Based on the univariable and multivariable models, the slope was the only parameter with a significant impact on the probability of obtaining an abnormal RGC+ map (odds ratio [OR] = 0.26; 95% CI = 0.08–0.80;  $P = 0.019$ ). Also, the multivariable



**Figure 3.** Distribution of (A) foveal width, (B) foveal depth, (C) foveal slope, and (D) age of the entire sample ( $N = 126$ ), showing where the values from the 12 eyes with circumfoveal artifacts fall.

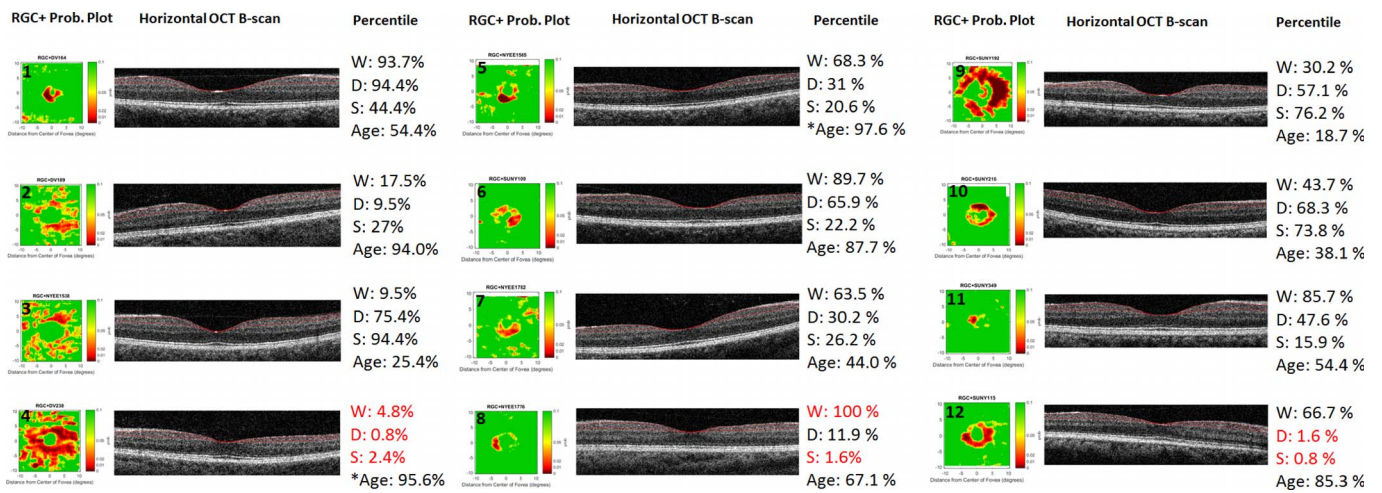


**Figure 4.** Macular RGC+ layer probability maps, b-scans, foveal parameters, and age of the 12 eyes with circumfoveal artifacts. Note that three of the 12 eyes fell outside the 95% CI on one or more of the three foveal morphologic parameters (all three for slope [S] and two for width [W] and depth [D]). Those three eyes are shown in the bottom row, the values in red depicting outliers for the three parameters. Only two of the 12 eyes fell outside the 95% CI for age. Those two eyes (maps 4 and 5) fell above the 95th percentile.

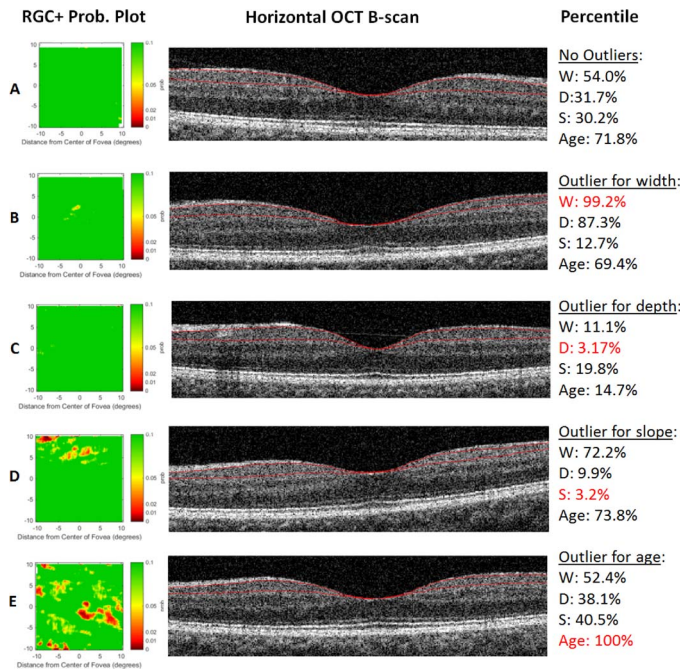


**Figure 5.** Macular RGC+ layer probability maps, b-scans, foveal parameters, and age for eyes with normal RGC+ plots (normal circumfoveal thickness). Plot (A) shows an eye with normal parameters while plots (B) to (E) show eyes that are outliers for width (W), depth (D), slope (S), and age despite having normal RGC+ plots.

model did significantly better than a null model (i.e., intercept only,  $P = 0.0108$ , Likelihood Ratio Test). However, the four parameters only accounted for 11% of the total variability (McFadden's pseudo- $R^2$ ).

## Discussion

We tested the hypothesis that variations in foveal morphology can account for artifacts seen on RGC+ probability maps in healthy subjects. First, we found

that 12 of the 126 (9.5%) healthy eyes tested with sdOCT macular cube scans had an abnormal circumfoveal RGC+ thickness map within the central 4°. However, only three of 12 (25%) eyes were outliers for at least one of the three predefined foveal morphologic parameters (width, depth, and slope). Finally, a regression model revealed that, despite a statistically significant effect of one parameter (slope), the full model explained only 11% total variability of having an abnormal circumfoveal RGC+ probability map. Therefore, despite suggesting a statistically-significant role of fovea morphology (i.e., slope) on the likelihood of having an abnormal macular scan, our findings do not support the premise that fovea morphology, as measured in this study, has a clinically-significant role explaining artifacts seen on macular scans. It is likely that variations in the distribution of RGC+ thickness are not reflected in our measures of foveal morphology.

To better interpret the result of macular scans for glaucoma diagnosis, it is important to understand the sources of variability and artifacts. In addition, we strongly recommend evaluating magnified b-scans to rule out retinal abnormalities, as well as to help distinguish between glaucoma versus other optic neuropathies.<sup>2,3</sup> With growing interest in the structure and function of the macula in glaucoma, clinicians are confronted more frequently with situations where the OCT results are confusing or inconsistent with other tests, such as visual fields or optic disc imaging. Despite new evidence that glaucomatous damage to the macula is more common than previously thought, overcalling macular damage due to artifacts seen on OCT can lead to misdiagnosis and unnecessary initiation or escalation of therapy.

Similar to what has been learned regarding the optic disc and its sources of variability (e.g., size and

**Table.** Results of the Binary Logistic Regression Testing the Association Between the Outcome Variable (Circumfoveal Artifacts: Yes vs. No) and the Set of Predictors (Foveal Width, Depth, Slope, and Subject's Age)

Parameter	Univariable			Multivariable		
	OR	95% CI	P Value	OR	95% CI	P Value
Width (per 10 $\mu\text{m}$ )	1.096	0.913	1.315	0.325		
Depth (per 10 $\mu\text{m}$ )	0.391	0.146	1.042	0.060		
Slope (per 0.1 $\mu\text{m}$ )	0.274	0.094	0.798	0.018*	0.265	0.087
Age (per decade)	1.390	0.921	2.097	0.117	1.380	0.899
					0.804	2.117
						0.019*
						0.140

The multivariable model was performed using a backward selection approach with the significance level of 0.20 for removal from the model.

\* Significant at  $P < 0.05$ .

shape), the macular anatomy also differs among subjects regarding newly identified parameters. Among these parameters, the width, depth, and slope of the foveal pit has a substantial range of values among healthy subjects (Fig. 3). The variation in these parameters could be the result, for example, of the density of RGCs within the macula. For a given area (e.g.,  $\pm 4^\circ$ ) some eyes may have a greater number of RGCs. This could explain differences in slope between the foveal pit and maxima of the internal limiting membrane. In fact, this was the only parameter associated statistically with an abnormal macular map. To assess the role of the density of RGCs within the macula on structure–function relationships, Turpin et al.<sup>22</sup> used a model based on the ratio of an individual’s RGC+ thickness to the population average. Their model revealed some asymmetry relative to the center of the fovea, which was fairly small in the nasal/temporal meridian, but greater in the superior/inferior meridian. Their results also demonstrated that although the average individual RGC displacement did not deviate from the population displacement, the variation among individuals was substantial. Based upon this work, Sepulveda et al.<sup>20</sup> showed that individually customized structure–function maps of the macula using predefined parameters (central thickness, maximum thickness, and radius) can predict individual differences and could help the investigation of glaucomatous damage in the macular region. Future studies ought to evaluate whether differences in slopes in the macula can influence structure–function relationships in that area.

Another important variable tested in our study was age, and this was based on the knowledge that neuronal density decreases with age in the population. Notwithstanding, it also is known that such decrease is less pronounced in the macula than in other parts of the retina (0.29%/y vs. 0.53%/y).<sup>30</sup> We found no significant effect of age on the likelihood of presenting an abnormal macular map. Studies have shown a very small effect of aging (measured longitudinally) on OCT-measured cpRNFL ( $-0.54 \mu\text{m}/\text{y}$ )<sup>20</sup> and macular ganglion cell complex (RNFL + RGC+,  $-0.92 \mu\text{m}/\text{y}$ ).<sup>31</sup> Based upon our study, age alone or in combination with other fovea anatomy parameters did not do well in explaining artifacts seen on sdOCT macular maps.

One limitation of our study is that it may be difficult to differentiate artifacts seen on RGC+ probability maps from true RGC+ loss, especially when they overlap. Nonetheless, it is important first

to understand what these artifacts look like in healthy subjects so that they are not confused with patterns more typical of glaucoma (i.e., arcuate defects in areas of vulnerability).<sup>2</sup> Future studies investigating the role of the foveal anatomy on the diagnostic performance (sensitivity and specificity) of macular maps as well as its influence on detecting progression are warranted.

## Acknowledgments

Presented in part at the 2015 Annual Meeting of the Association for Research in Vision and Ophthalmology, Denver, Colorado, United States.

Supported by an unrestricted departmental grant from Research to Prevent Blindness, New York, NY, USA (Department of Ophthalmology, Columbia University Medical Center); National Institutes of Health/National Eye Institute (NIH/NEI; Bethesda, MD) Grants EY02115 (DCH) and EY025253 (CGDM).

Disclosure: **C.G. De Moraes**, None; **H. Muhammad**, None; **K. Kaur**, None; **D. Wang**, None; **R. Ritch**, None; **D.C. Hood**, None

## References

1. Zhang L, Drance SM, Douglas GR. Automated perimetry in detecting threats to fixation. *Ophthalmology*. 1997;104:1918–1920.
2. Hood DC, Raza AS, De Moraes CG, Liebmann JM, Ritch R. Glaucomatous damage of the macula. *Prog Retin Eye Res*. 2013;32:1–21.
3. Hood DC. Improving our understanding, and detection, of glaucomatous damage: an approach based upon optical coherence tomography (OCT). *Prog Retin Eye Res*. 2017;57:46–75.
4. De Moraes CG, Hood DC, Thenappan A, et al. 24-2 Visual fields miss central defects shown on 10-2 tests in glaucoma suspects, ocular hypertensives, and early glaucoma. *Ophthalmology*. 2017; 124:1499–1456.
5. Wang DL, Raza AS, De Moraes CG, et al. Central glaucomatous damage of the macula can be overlooked by conventional oct retinal nerve fiber layer thickness analyses. *Trans Vis Sci Tech*. 2015;4:4.

6. Grillo LM, Wang DL, Ramachandran R, et al. The 24-2 visual field test misses central macular damage confirmed by the 10-2 visual field test and optical coherence tomography. *Trans Vis Sci Tech.* 2016;5:15.
7. Sullivan-Mee M, Karin Tran MT, Pensyl D, Tsan G, Katiyar S. Prevalence, features, and severity of glaucomatous visual field loss measured with the 10-2 achromatic threshold visual field test. *Am J Ophthalmol.* 2016;168:40–51.
8. Park HY, Hwang BE, Shin HY, Park CK. Clinical clues to predict the presence of parafoveal scotoma on Humphrey 10-2 visual field using a Humphrey 24-2 visual field. *Am J Ophthalmol.* 2016;161:150–159.
9. Zhang X, Dastiridou A, Francis BA, et al. Baseline Fourier-domain optical coherence tomography structural risk factors for visual field progression in the advanced imaging for glaucoma study. *Am J Ophthalmol.* 2016;172:94–103.
10. Belghith A, Medeiros FA, Bowd C, et al. Structural change can be detected in advanced-glaucoma eyes. *Invest Ophthalmol Vis Sci.* 2016;57:511–518.
11. Rao HL, Begum VU, Khadka D, Mandal AK, Senthil S, Garudadri CS. Comparing glaucoma progression on 24-2 and 10-2 visual field examinations. *PLoS One.* 2015;10:e0127233.
12. Traynis I, De Moraes CG, Raza AS, Liebmann JM, Ritch R, Hood DC. Prevalence and nature of early glaucomatous defects in the central 10 degrees of the visual field. *JAMA Ophthalmol.* 2014;132:291–297.
13. Kim YK, Ha A, Na KI, Kim HJ, Jeoung JW, Park KH. Temporal relation between macular ganglion cell-inner plexiform layer loss and peripapillary retinal nerve fiber layer loss in glaucoma. *Ophthalmology.* 2017;124:1056–1064.
14. Hood DC, Raza AS, De Moraes CG, et al. Initial arcuate defects within the central 10 degrees in glaucoma. *Invest Ophthalmol Vis Sci.* 2011;52:940–946.
15. Girkin CA, Liebmann J, Fingeret M, Greenfield DS, Medeiros F. The effects of race, optic disc area, age, and disease severity on the diagnostic performance of spectral-domain optical coherence tomography. *Invest Ophthalmol Vis Sci.* 2011;52:6148–6153.
16. Hood DC, Salant JA, Arthur SN, Ritch R, Liebmann JM. The location of the inferior and superior temporal blood vessels and interindividual variability of the retinal nerve fiber layer thickness. *J Glaucoma.* 2010;19:158–166.
17. Knighton RW, Gregori G, Budenz DL. Variance reduction in a dataset of normal macular ganglion cell plus inner plexiform layer thickness maps with application to glaucoma diagnosis. *Invest Ophthalmol Vis Sci.* 2012;53:3653–3661.
18. Knighton RW, Gregori G. The shape of the ganglion cell plus inner plexiform layers of the normal human macula. *Invest Ophthalmol Vis Sci.* 2012;53:7412–7420.
19. Dubis AM, McAllister JT, Carroll J. Reconstructing foveal pit morphology from optical coherence tomography imaging. *Br J Ophthalmol.* 2009;93:1223–1227.
20. Sepulveda JA, Turpin A, McKendrick AM. Individual differences in foveal shape: feasibility of individual maps between structure and function within the macular region. *Invest Ophthalmol Vis Sci.* 2016;57:4772–4778.
21. Raza AS, Cho J, De Moraes CG, et al. Retinal ganglion cell layer thickness and local visual field sensitivity in glaucoma. *Arch Ophthalmol.* 2011;129:1529–1536.
22. Turpin A, Chen S, Sepulveda JA, McKendrick AM. Customizing structure-function displacements in the macula for individual differences. *Invest Ophthalmol Vis Sci.* 2015;56:5984–5989.
23. Hood DC, Raza AS. On improving the use of OCT imaging for detecting glaucomatous damage. *Br J Ophthalmol.* 2014;98(suppl 2):ii1–9.
24. Hood DC, Raza AS, De Moraes CG, et al. Evaluation of a one-page report to aid in detecting glaucomatous damage. *Trans Vis Sci Tech.* 2014;3:8.
25. Williams DR. Visual consequences of the foveal pit. *Invest Ophthalmol Vis Sci.* 1980;19:653–667.
26. Hood DC, Cho J, Raza AS, Dale EA, Wang M. Reliability of a computer-aided manual procedure for segmenting optical coherence tomography scans. *Optom Vis Sci.* 2011;88:113–123.
27. Ctori I, Huntjens B. The association between foveal morphology and macular pigment spatial distribution: an ethnicity study. *PLoS One.* 2017;12:e0169520.
28. Liu L, Marsh-Tootle W, Harb EN, et al. A sloped piecemeal Gaussian model for characterising foveal pit shape. *Ophthalm Physiol Optics.* 2016;36:615–631.
29. Kirby ML, Galea M, Loane E, Stack J, Beatty S, Nolan JM. Foveal anatomic associations with the secondary peak and the slope of the macular pigment spatial profile. *Invest Ophthalmol Vis Sci.* 2009;50:1383–1391.

30. Harman A, Abrahams B, Moore S, Hoskins R. Neuronal density in the human retinal ganglion cell layer from 16-77 years. *Anat Rec.* 2000;260:124–131.
31. Shoji T, Zangwill LM, Akagi T, et al. Progressive macula vessel density loss in primary open angle glaucoma: a longitudinal study. *Am J Ophthalmol.* 2017;182:107–117.